Journal of Magnetic Resonance 209 (2011) 244–249

Contents lists available at ScienceDirect

Journal of Magnetic Resonance

journal homepage: www.elsevier.com/locate/jmr

Sequential CW-EPR image acquisition with 760-MHz surface coil array

Ayano Enomoto, Hiroshi Hirata *

Division of Bioengineering and Bioinformatics, Graduate School of Information Science and Technology, Hokkaido University, North 14, West 9, Kita-ku, Sapporo 060-0814, Japan

ARTICLE INFO

Article history:
Received 1 December 2010
Revised 19 January 2011
Available online 26 January 2011

Keywords:
Surface coil
Array
Decoupling
CW-EPR imaging

ABSTRACT

This paper describes the development of a surface coil array that consists of two inductively coupled surface-coil resonators, for use in continuous-wave electron paramagnetic resonance (CW-EPR) imaging at 760 MHz. To make sequential EPR image acquisition possible, we decoupled the surface coils using PIN-diode switches, to enable the shifting of the resonators resonance frequency by more than 200 MHz. To assess the effectiveness of the surface coil array in CW-EPR imaging, two-dimensional images of a solution of nitroxyl radicals were measured with the developed coil array. Compared to equivalent single coil acquired images, we found the visualized area to be extended approximately 2-fold when using the surface coil array. The ability to visualize larger regions of interest through the use of a surface coil array, may offer great potential in future EPR imaging studies.

1. Introduction

Electron paramagnetic resonance (EPR) imaging is an important technique to detect free radicals in subject animals noninvasively [1]. It is widely recognized that free radicals are associated with many diseases, such as inflammation and ischemia/reperfusion injury [2,3]. Therefore, the visualization of the distribution of free radicals in small animals is useful to understand the mechanisms of free-radical-related diseases. In EPR imaging, typically two types of resonators have been used, namely, volume-coil [4–9] and surface-coil resonators [10–12]. The dimensions of the coils are small in comparison to the wavelength of the operation frequencies of *in vivo* EPR spectroscopy and imaging, which typically range from 250 MHz to 1.2 GHz [13,14]. This frequency range is chosen to allow sufficient penetration in biological tissue, and to minimize tissue heating due to RF absorption. However this requirement is a compromise with the need to obtain higher sensitivity, which is generally achieved with higher microwave frequencies [15]. To overcome the constraints of resonator size imposed by frequency requirements, Petryakov et al. developed a larger surface-coil resonator with a 1.1 GHz operation frequency, by combining four identical loop segments [16]. Similarly, phased-array coils have been utilized in proton magnetic resonance imaging (MRI) [17–19], and applied clinically for visualization of large regions of interest such as human spine [20]. However, one of the main obstacles to the use of the arrayed coil design in MRI and EPR imaging, is the need to suppress the mutual coupling, or inductive interaction of the coils [21].

Preliminary surface coil array designs for continuous-wave (CW) EPR imaging, are similar to MRI coil arrays in that they are both designed to extend the area of visualization, however there are a number of fundamental differences between MRI and CW-EPR scanning techniques, primarily related to the method of signal detection. As such, in developing surface coil arrays for CW-EPR imaging, the following considerations must be addressed:

(i) The imaging sample and the resonator(s) are exposed to magnetic field modulation in CW-EPR detection. MRI does not use low frequency (~100 kHz) magnetic field modulation. Therefore, decoupling circuits should be situated away from region of magnetic field modulation to avoid interference at low modulation frequencies.
(ii) Since the resonator is constantly driven in CW-EPR imaging, the microwave carrier frequency or the resonance frequency of the resonator(s) should be controlled to make the reflected microwaves from the resonator minimal by a negative feedback control system.

The goal of our work was to demonstrate the feasibility of the surface coil array for CW-EPR imaging that can extend the area of visualization of the surface coils. By shifting the resonance frequency of one of the surface-coil resonators with a PIN-diode switch, we were able to suppress mutual coupling and extend the area of visualization of EPR imaging.

2. Methods

2.1. Sequential image acquisition

As illustrated in Fig. 1, the surface coil array consists of two surface-coil resonators and two kinds of switches, i.e., RF coaxial (919C70100, Transco Products Inc., Camarillo, CA) and PIN-diode

* Corresponding author. Fax: +81 11 706 6762.
E-mail address: hhirata@ist.hokudai.ac.jp (H. Hirata).

1090-7807/$ - see front matter © 2011 Elsevier Inc. All rights reserved.
doi:10.1016/j.jmr.2011.01.021

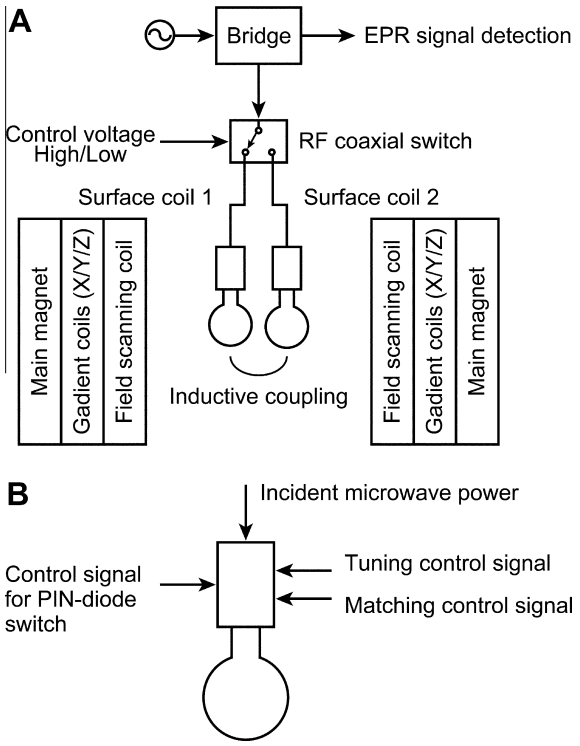

Fig. 1. Schematic diagram of surface coil array and a CW-EPR spectrometer. (A) Configuration of two surface coils and an RF coaxial switch. (B) Input signals applied to an individual surface coil.

switches. When the PIN-diode switch in the resonator circuit is turned on, the resonance frequency of the resonator is shifted, thereby suppressing the mutual coupling due to the difference in the resonance frequencies of the two circuits. EPR data acquisition was sequentially performed for each resonator, such that when obtaining measurements with the first resonator, microwaves were not fed to the second resonator. This was achieved using low resistance PIN-diodes, causing a shift in the resonance frequency of the second resonator. After imaging with the first resonator, the process was repeated by connecting the second resonator to the EPR bridge, allowing images to be acquired with the second resonator.

2.2. Surface coil array

Fig. 2 shows the configuration of the surface-coil resonator. The LC resonance circuit was driven through a parallel transmission line, with a matching circuit using varactor diodes connected in parallel to the transmission line [22,23]. Frequency adjustment was achieved by changing the capacitive reactance using varactor diodes connected in series to the transmission line. The development of the resonator was based largely on a previously reported 300 MHz loop resonator [23], with the addition of electronic tuning and matching control functions, which have previously been used in CW-EPR spectrometers [8,24–27]. The substrate of the surface coils was made from copper laminate (DiClad 880, Arlon Inc., Santa Ana, CA), and for impedance matching, frequency tuning, and PIN-diode switch circuits, another substrate was used (FR-4, Sunhayato, Tokyo, Japan). The copper laminate on the backside of the substrate of the surface coils was removed, and several coil arrays were constructed, with a coil inner diameter and width of 7 mm and 2 mm respectively. The constructed arrays were fixed onto the substrate, in each case with varying distances between the centers of two coils ranging from 4 mm to 7 mm, resulting in a partial overlap of the coils. To assess the characteristics of the surface coil array when distances between the centers of the coils were greater than 7 mm, two separately fabricated, non-overlapping coils were used. To electrically insulate the coils from each other, polytetrafluoroethylene sheets were inserted into the overlapping regions. The non-magnetic chip capacitors (11-2R2-C-1000-S for 2.2 pF, 11-4R7-C-1000-S for 4.7 pF, Voltronics, Denville, NJ) were used in the tuning and impedance matching circuit to prevent the effect of magnetic field modulation. When the surface coils are exposed to magnetic field modulation, an electromotive force (emf) is generated at the frequency of field modulation. If the emf is transferred to the tuning and matching circuits through the coaxial transmission lines, the reverse-bias voltage applied to the varactor diodes is modulated at the frequency of field modulation and it leads to a shift in the resonance frequency and the reflection of the incident microwaves at the resonator. This effect causes a shift in the baseline of detected EPR spectra. To prevent this unwanted effect of magnetic field modulation, we connected low value capacitors (2.2 pF) in series between the transmission lines and the varactor diodes. Because these capacitors have large impedance at the frequency of field modulation (90 kHz), the emf due to magnetic field modulation cannot be transferred to the varactor diodes.

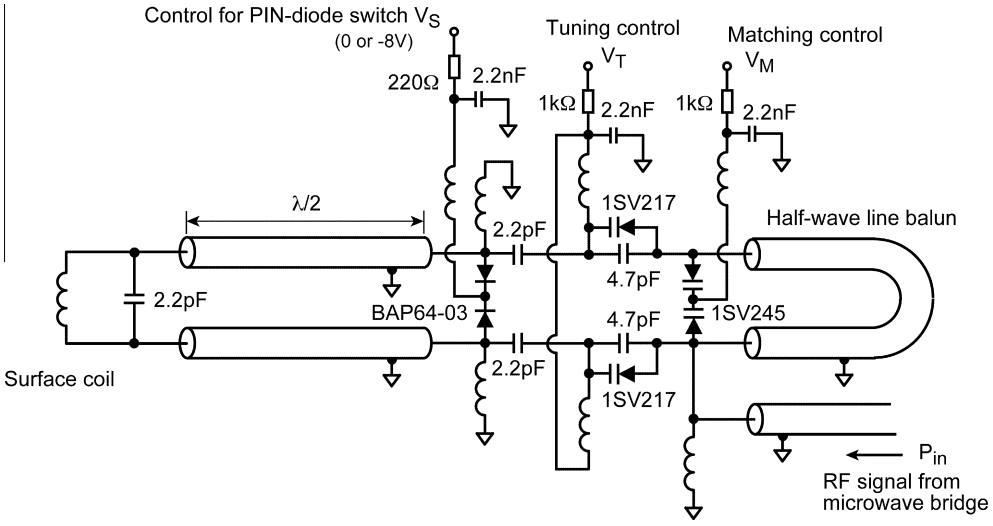

Fig. 2. Circuitry diagram of individual surface coil. The PIN-diode switch becomes a low-impedance when the negative voltage (−8 V) is applied to the control port V_S. Decoupling of the coils is achieved by changing the negative voltage on (−8 V) and off (0 V).

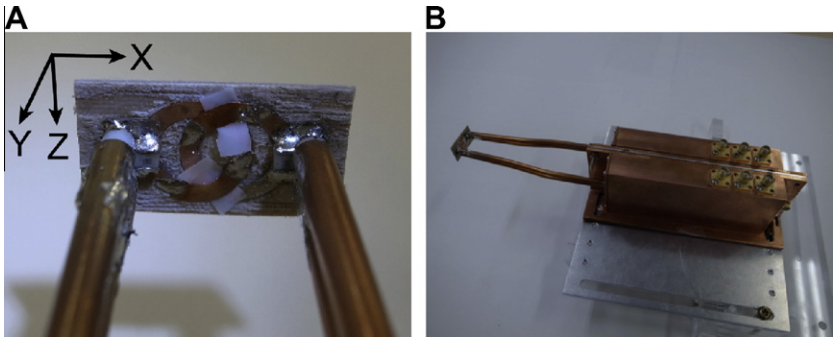

Fig. 3. Photographs of surface coils (A) and whole structure of the prototype coil array (B).

To adjust the tuning and impedance matching electronically, varactor diodes (1SV217 for the tuning circuit, 1SV245 for the matching circuit, Toshiba, Tokyo, Japan) were used in both the tuning and matching circuits. For adjustment of impedance matching, the reverse-bias voltage applied to the varactor diodes was changed. The resonance frequencies of the resonators were adjusted to the microwave carrier frequency, where the adjustable range of the resonance frequency of the resonator was approximately 8 MHz. PIN-diodes (BAP64-03, Royal Philips Electronics, Netherland) were used for shifting the resonance frequency of the resonator to decouple the surface coils. By placing PIN-diodes between the coaxial lines (Fig. 2) and applying a negative voltage, the transmission line was shorted due to the low resistance of the PIN-diodes. Thus, the resonance frequency of the resonator was significantly altered due to the change in resonance circuit properties. The parallel transmission line and the half-wave line balun were made from semi-rigid coaxial cables (3.6 mm in diameter and characteristic impedance of 50 Ω, SX-36, Sanken Corp., Tokyo, Japan). The return loss and the quality factor of each resonator were measured with a network analyzer (E5062A, Agilent Technologies, Palo Alto, CA) to check the operation of the surface coil array.

In Fig. 3A and B, the two coils and the complete resonator construction are pictured respectively. Each coil was connected to the end of the transmission line. The frequency tuning and impedance matching circuits were encased in copper housing to prevent interference due to magnetic field modulation, and aluminum plates were inserted into the gap of the resonators to adjust the distance between the coils. The entire length of the resonators including the shielding box was 236 mm. Since the diameter of the coils for magnetic field modulation was 100 mm and the length of the transmission line (half-wave line) was 126 mm, the copper shielding case was a sufficient distance from the region of magnetic field modulation and outside of the static magnetic field, thus avoiding problems associated with the generation of eddy currents.

2.3. Frequency and impedance matching adjustment

To make sequential measurements easier, impedance matching and frequency tuning of the individual resonators were adjusted in advance. The resonance frequencies of the resonators have to be tuned in the lock-in range of automatic tuning control (ATC). However, it is difficult to make multiple resonators with identical characteristics. Since the ATC system can adjust only one resonator, we built an electrical circuit that selects the resonator being adjusted in terms of its frequency and impedance matching. Fig. 4A illustrates a block diagram of the electrical circuits of the frequency and impedance matching adjustment, while in Fig. 4B the summing amplifier used for the frequency tuning of the resonators is schematically shown. On the right side of the summing amplifier, we employed a compensator (lag-lead filter) to prevent the unwanted oscillation of the feedback loop in ATC [28]. Before the measurements, the impedance matching of each resonator was adjusted to the 50-Ω coaxial line connected to the EPR bridge.

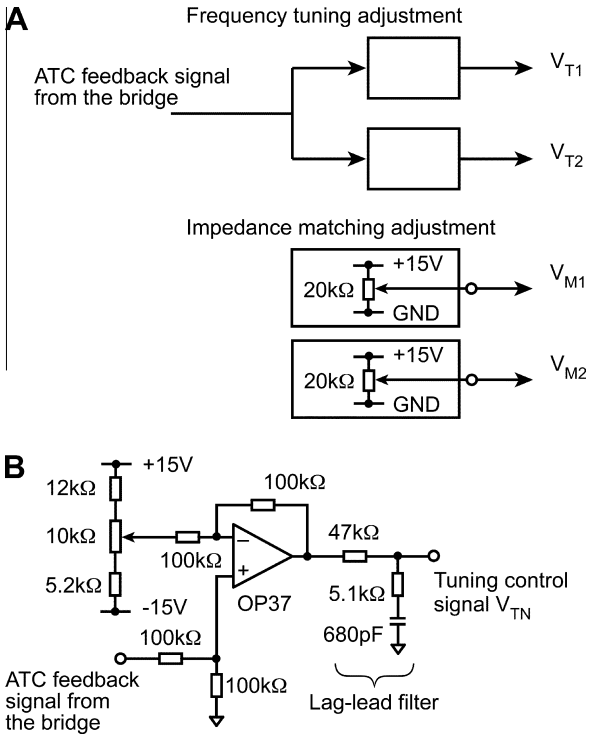

Fig. 4. Diagram of voltage adjustment circuits. (A) Block diagram of the adjustment for tuning and matching control voltages. (B) Voltage adjustment circuit for frequency tuning.

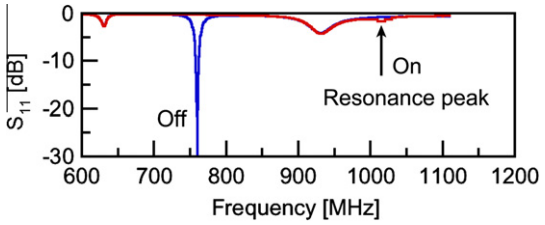

Fig. 5. Typical scattering-matrix parameter S_{11} for an individual surface-coil resonator when the PIN-diode switch was off and on.

2.4. EPR imager and image reconstruction

A previously reported laboratory-built 750-MHz CW-EPR imager [29,30] was used in the experiments, consisting of a set of 3D

field gradient coils, with a 60 mm gap between the two magnets. We used a Helmholtz coil pair with a 50 mm gap as a modulation coil and placed it between the magnets. After acquiring EPR spectra with both resonators, two-dimensional (2D) images were individually reconstructed on the basis of the filtered back-projection algorithm [31], and the reconstructed images were combined to form the final image using the "Add" function of ImageJ software (National Institutes of Health, Bethesda, MD) [32].

2.5. Phantom imaging

To investigate the area of visualization of the surface coil array, we measured 2D EPR images of a glass cell phantom ($10 \times 10 \times 45$ mm) filled with 4.5 mL of a solution of 1 mM 4-hydroxy-2,2,6,6-tetramethylpiperidine-d_{17}-1-^{15}N-oxyl (TEMPOL-d_{17}-^{15}N). The distance between the centers of two coils was varied from 4 mm to 7 mm, with a field-of-view (FOV) set to 40 mm. The parameters for EPR imaging were as follows: scanning field 2.0 mT, magnetic field gradient 50 mT/m, magnetic field modulation 0.15 mT, modulation frequency 90 kHz, scan time 1.0 s, time constant 0.3 ms, applied microwave power 20 mW, number of projections 32, with five averages, giving a total image acquisition time of 3 min.

3. Results

3.1. Decoupling of coils

Fig. 5 shows the characteristics of return loss (scattering-matrix parameter S_{11}) measured for an individual surface-coil resonator when the PIN-diode switch was off and on. As shown in Fig. 5, the resonance frequency of the resonator was shifted from 760 MHz to 1.01 GHz when the PIN-diode switch was turned on (the status of low resistance). When the resonance frequencies of the two coils are significantly different from each other, the impedance of the each coil in a non-resonant condition is sufficiently high enough that minimal interaction between the two resonant circuits occurs, even if the two coils are situated in close proximity to each other. This is the basis by which the PIN-diode switch is used to decouple the surface coils.

Fig. 6 shows the typical traces of the return loss of an individual surface coil. As shown in Fig. 6A, when the PIN-diode switch of one of two resonators was off, dual-peak resonance appeared, due to the effect of mutual coupling between two coils. Whereas the resonance frequency of the coil that was not driven by the EPR bridge, was shifted more than 200 MHz when the PIN-diode switch of one of two resonators was on, giving a single resonance peak as shown in Fig. 6B. This result demonstrates the effectiveness of using the PIN-diode switch (Fig. 2) for the suppression of mutual coupling.

Fig. 7A and B shows the characteristics of the resonance peaks when the distance between the centers of the two coils was varied in a lateral direction (the *X*-direction in Fig. 3A), with the resonance frequency of the resonators set to 760 MHz, for PIN-diode off and on conditions respectively. As shown in Fig. 7A, under the presence of the mutual coupling, the dual-peak resonance appeared and the frequencies of their peaks deviated away from 760 MHz. When the distance between the two coils was closer, the difference in the frequencies of their peaks was larger. The emf generated is proportional to the rate of change of the magnetic flux (Faraday's law). When the distance between the two coils was increased, the flux through the coil became smaller, resulting in a smaller motional emf and therefore less mutual inductance between the two coils. Because the frequency response curve of inductively coupled resonance circuits (i.e., transformer coupling circuits) depends on the amount of coupling [33], the frequencies of the dual-peak response

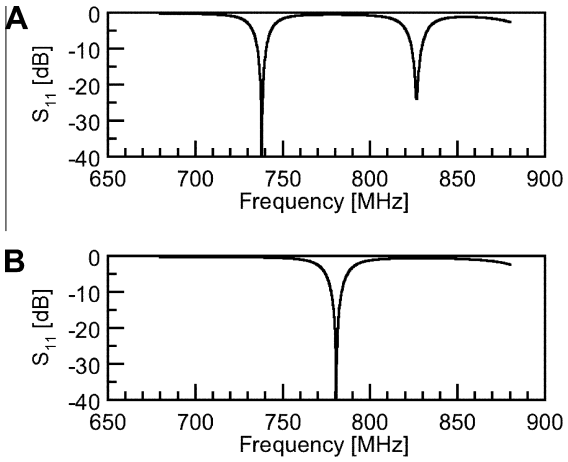

Fig. 6. Typical scattering-matrix parameter S_{11} for one of the two resonators in the surface coil array when the PIN-diode switch was off (A) and on (B).

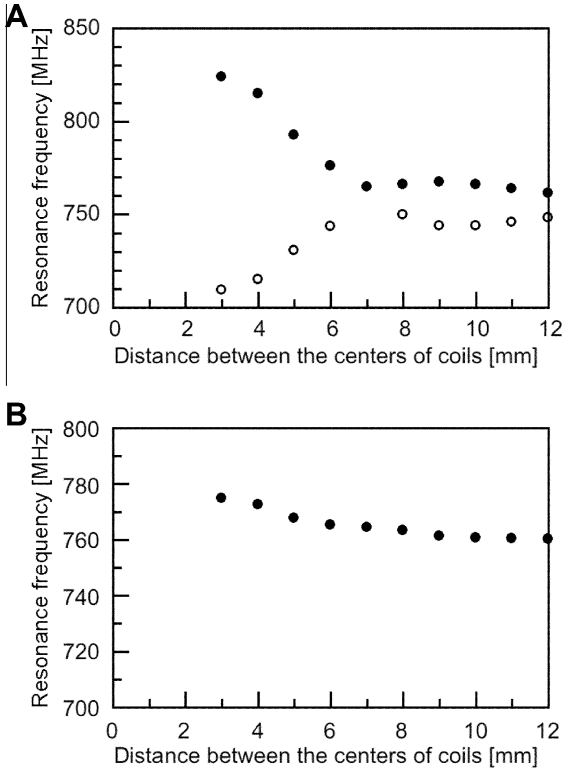

Fig. 7. A shift in the resonance frequencies for (A) inductively coupled surface coil and (B) decoupled surface coil. For dual-peak resonance, the frequencies of upper peak (closed circle) and lower peak (open circle) are plotted as a function of the distance between the centers of the coils in (A). For the decoupled coil, a single peak of resonance appeared, and its resonance frequency was plotted in (B).

vary as a function of the distance between the two coils. However, when the distance between the centers of the coils was 7 mm, the resonance peaks appeared at the same frequency, suggesting an apparent absence of mutual coupling. When positioned at this specific distance, the mutual inductance of the adjacent coils becomes zero, thereby eliminating the problem of dual-peak resonance for the inductively coupled resonant circuits [17]. This result is consistent with previous work in NMR array coils. On the other hand, as shown in Fig. 7B, when the PIN-diode switch was on and the mutual coupling was suppressed, the single resonance peak appeared close to the resonance frequency of 760 MHz, irrespective of the

Table 1
Quality factor of individual surface-coil resonators.

Distance between coils [mm]	Quality factor	
	Resonator 1	Resonator 2
4	102	100
5	110	105
6	111	107
7	110	104

distance between the coils with a maximum frequency difference less than 15 MHz, which decreased as the distance between the coils was increased. Table 1 lists the unloaded quality factors of the resonators. The voltage of frequency tuning was set to 8 V, when those parameters were measured.

3.2. Images measured with surface coil array

To investigate the area of visualization of the surface coil array, we measured a glass cell phantom (Fig. 8A). Fig. 8B shows 2D EPR images of the phantom, acquired with a single coil in *XY*- and *XZ*-planes. Fig. 8C and D shows the combined EPR images measured with the surface coil array, with varying distances between centers of the coils. When the distance between the centers of two coils was 7 mm, the distribution of signal intensity was not uniform in both planes. When the distance of coils was greater than 7 mm, the area of visualization was split into two areas that correspond to two non-overlapping coils. In the *XZ*-plane, the area of visualization was approximately equal to the inner area of the coils, with signal intensity enhancement near the center of each image due to the lens effect [34,35]. The images in the *XY*-plane show the sensitivity of depth to be approximately 3 mm in each distance.

4. Discussion

The experimental results showed that the surface coil array could extend the area of visualization in CW-EPR imaging. The area of visualization with the surface coil array was extended approximately 2-fold in comparison to that of a conventional surface coil. In our experimental results, a drop in the signal intensity of the EPR image in Fig. 8C and D was observed when the distance between the centers of two coils was 7 mm. This is because the area of visualization for each coil is limited. If there is no overlapping area of visualization in the array coil system, we cannot obtain a continuous area of visualization between the two coils. Although the microwave characteristics of the medium surrounding the coils affects the RF magnetic field distribution, the results in Fig. 8 demonstrate the feasibility of the surface coil array in CW-EPR imaging.

One of the important technical issues regarding the surface coil array was decoupling of the coils. The PIN-diode switches in the resonators could suppress the mutual coupling of the coils. However, the resonance frequency was slightly shifted when the PIN-diode switch was turned on, because the mutual coupling of coils could not be removed completely. Decoupling techniques of coil arrays have previously been investigated in MRI [36,37], and although modern MRI methods are based on a pulsed protocol, knowledge of decoupling techniques regarding coil arrays can also be applied in CW-EPR imaging. This may become increasingly relevant for future work, where decoupling techniques for an increased number of coils will be a key technical challenge.

A shift in the resonance frequency of more than 200 MHz was observed when using our surface coil array with the PIN-diode switch was on. Since this shift in the frequency was enough to decouple the coils, the dual-peak resonance disappeared, as illustrated in Fig. 6A and B. Similarly, Yokoyama investigated the twin-loop resonator system at 245 MHz [38]. While dual-peak resonance appeared in the two-loop resonator system, it was suppressed with a combination of a phase shifter and a power combiner. Two coils were excited together in the twin resonator system.

When the area of visualization was extended, the signal-to-noise ratios of the reconstructed images were not sacrificed regardless of the position of the surface coils. This is because the data acquisition of EPR spectra under magnetic field gradients was performed with each coil sequentially, and the effect of mutual coupling between the two coils was suppressed by shifting the resonance frequency of the resonator, which was not fed. Thus, the signal-to-noise ratios of the obtained images depend on the sensitivity of each resonator. In our experimental setup, the efficiency of each resonator in generating RF magnetic fields was similar to that of a conventional, single surface-coil resonator.

In future work, the following technical issues regarding the use of the surface coil array in CW-EPR imaging will need to be addressed: (i) The variation of the resonance frequencies of individual resonators should be less than several MHz. This was constrained with the characteristics of ATC. In our preliminary experiments, we could not perform measurements when the difference in resonator frequencies was greater than 5 MHz, because each resonator could not be tuned to the microwave carrier frequency. (ii) Bulky shielding cases should be re-designed to accommodate a set of tuning and matching circuits for a number of surface coils.

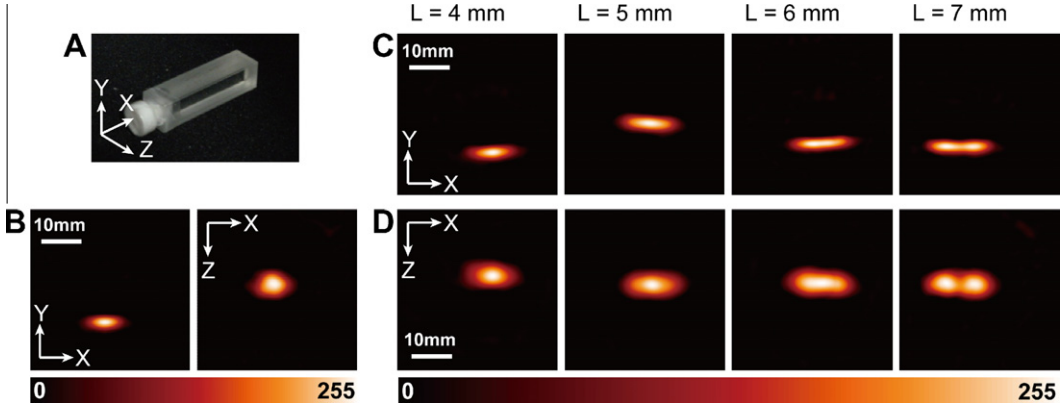

Fig. 8. EPR images of nitroxyl radicals measured with a surface coil array. (A) Photograph of the glass cell used as a phantom. It was filled with 1 mM TEMPOL-d_{17}-^{15}N solution. (B) 2D EPR images measured with a single surface coil. Measured 2D EPR images with the surface coil array in the *XY*-plane (C) and the *XZ*-plane (D). The distance (*L*) between the centers of the coils was changed. The surface coil array was placed on the glass cell filled with a solution of 1 mM TEMPOL-d_{17}-^{15}N.

5. Conclusions

We demonstrated the feasibility of using a surface coil array in CW-EPR imaging. Our prototype showed good suppression of the mutual coupling of the coils in CW-ERP detection. Our results highlight fundamental characteristics of the surface coil array in CW-EPR imaging, in particular the increased region of visualization that is attainable when compared to conventional surface coils, which may be particularly beneficial for the imaging of free radical distribution in small animals.

Acknowledgments

The authors are grateful to Dr. Jonathan Goodwin for a critical reading of the manuscript. This work was supported by SENTAN, JST.

References

[1] H.M. Swartz, L.J. Berliner, Introduction to in vivo EPR, in: L.J. Berliner (Ed.), Biological Magnetic Resonance, vol. 18, Kluwer Academic/Prenum Publishers, New York, 2003, pp. 1–20.
[2] S. Cuzzocrea, D.P. Riley, A.P. Caputi, D. Salvemini, Antioxidant therapy: a new pharmacological approach in shock, inflammation, and ischemia/reperfusion injury, Pharmacol. Rev. 53 (2001) 135–159.
[3] J.L. Zweier, M.A.H. Talukder, The role of oxidants and free radicals in reperfusion injury, Cardiovasc. Res. 70 (2006) 181–190.
[4] W. Froncisz, J.S. Hyde, The loop-gap resonator: a new microwave lumped circuit ESR sample structure, J. Magn. Reson. 47 (1982) 515–521.
[5] H.J. Halpern, D.P. Spencer, J. van Polen, M.K. Bowman, A.C. Nelson, E.M. Dowey, B.A. Teicher, Imaging radio-frequency electron-spin-resonance spectrometer with high-resolution and sensitivity for in vivo measurements, Rev. Sci. Instrum. 60 (1989) 1040–1050.
[6] P. Kuppusamy, M. Chzhan, K. Vij, M. Shteynbuk, D.J. Lefer, E. Giannella, J.L. Zweier, Three-dimensional spectral spatial EPR imaging of free-radicals in the heart – a technique for imaging tissue metabolism and oxygenation, Proc. Natl. Acad. Sci. USA 91 (1994) 2292–3388.
[7] M. Afeworki, G.M. van Dam, N. Devasahayam, R. Murugesan, J. Cook, D. Coffin, J.H. A.-Larsen, J.B. Mitchell, S. Subramanian, M.C. Krishna, Three-dimensional whole body imaging of spin probes in mice by time-domain radiofrequency electron paramagnetic resonance, Magn. Reson. Med. 43 (2000) 375–382.
[8] J.A. Brivati, A.D. Stevens, M.C.R. Symons, A radiofrequency ESR spectrometer for in vivo imaging, J. Magn. Reson. 92 (1991) 480–489.
[9] S. Ishida, S. Matsumoto, H. Yokoyama, N. Mori, H. Kumashiro, N. Tsuchihashi, T. Ogata, M. Yamada, M. Ono, T. Kitajima, H. Kamada, E. Yoshida, An ESR-CT imaging of the head of a living rat receiving an administration of a nitroxide radical, Magn. Reson. Imaging 10 (1992) 109–114.
[10] G. He, S.P. Evalappan, H. Hirata, Y. Deng, S. Petryakov, P. Kuppusamy, J.L. Zweier, Mapping of the B_1 field distribution of a surface coil resonator using EPR imaging, Magn. Reson. Med. 48 (2002) 1057–1062.
[11] S. Petryakov, M. Chzhan, A. Samouilov, G. He, P. Kuppusamy, J.L. Zweier, A bridged loop-gap S-band surface resonator for topical EPR spectroscopy, J. Magn. Reson. 151 (2001) 124–128.
[12] A.D. Stevens, A moderately sized resonator/surface coil for radiofrequency electron paramagnetic resonance spectroscopy and imaging in vivo, Br. J. Radiol. 67 (1994) 1243–1248.
[13] B.B. Williams, H.J. Halpern, In vivo EPR imaging, in: S.S. Eaton, G.R. Eaton, L.J. Berliner (Eds.), Biological Magnetic Resonance, vol. 23, Kluwer Academic/Prenum Publishers, New York, 2005, pp. 283–319.
[14] G.R. Eaton, S.S. Eaton, EPR spectrometers at frequencies below X-band, in: C.J. Bender, L.J. Berliner (Eds.), Biological Magnetic Resonance, vol. 21, Kluwer Academic/Prenum Publishers, New York, 2004, pp. 59–114.
[15] G.A. Rinard, R.W. Quine, S.S. Eaton, G.R. Eaton, Frequency dependence of EPR sensitivity, in: C.J. Bender, L.J. Berliner (Eds.), Biological Magnetic Resonance, vol. 21, Kluwer Academic/Prenum Publishers, New York, 2004, pp. 115–154.
[16] S. Petryakov, A. Samouilov, M. Chzhan-Roytenberg, E. Kesselring, Z.Q. Sun, J.L. Zweier, Segmented surface coil resonator for in vivo EPR applications at 1.1 GHz, J. Magn. Reson. 198 (2008) 8–14.
[17] P.B. Roemer, W.A. Edelstein, C.E. Hayes, S.P. Souza, O.M. Mueller, The NMR phased array, Magn. Reson. Med. 16 (1990) 192–225.
[18] W.E. Kwok, J. Zhong, Z. You, G. Seo, S.M.S. Totterman, A four-element phased array coil for high resolution and parallel MR imaging of the knee, Magn. Reson. Imaging 21 (2003) 961–967.
[19] K.V. Mogatadakala, J.A. Bankson, P.A. Narayana, Three-element phased-array coil for imaging of rat spinal cord at 7T, Magn. Reson. Med. 60 (2008) 1498–1505.
[20] G.J.L.A. Nijeholt, M.A.A. van Walderveen, J.A. Castelijns, J.H.T.M. van Waesberghe, C. Polman, P. Scheltens, P.F.W.M. Rosier, P.J.H. Jongen, F. Barkhof, Brain and spinal cord abnormalities in multiple sclerosis – correlation between MRI parameters, clinical subtypes and symptoms, Brain 121 (1998) 687–697.
[21] C. von Morze, J. Tropp, S. Banerjee, D. Xu, K. Karpodinis, L. Carvajal, C.P. Hess, P. Mukherjee, S. Majumdar, D.B. Vigneron, An eight-channel, nonoverlapping phased array coil with capacitive decoupling for parallel MRI at 3 T, Concept Magn. Reson. B Magn. Reson. Eng. 31B (2007) 37–43.
[22] G.A. Rinard, R.W. Quine, S.S. Eaton, G.R. Eaton, Microwave coupling structures for spectroscopy, J. Magn. Reson. Ser. A 105 (1993) 137–144.
[23] H. Hirata, G. He, Y. Deng, I. Salikhov, S. Petryakov, J.L. Zweier, A loop resonator for slice-selective in vivo EPR imaging in rats, J. Magn. Reson. 190 (2008) 124–134.
[24] H. Hirata, T. Walczak, H.M. Swartz, Electronically tunable surface-coil-type resonator for L-band EPR spectroscopy, J. Magn. Reson. 142 (2000) 159–167.
[25] S. McCallum, F. Resmer, Automatic coupling control system for radio frequency in vivo electron paramagnetic resonance based on a piezoelectric controlled capacitor, Rev. Sci. Instrum. 70 (1999) 4706–4710.
[26] M. Chzhan, P. Kuppusamy, J.L. Zweier, Development of an electronically tunable L-band resonator for EPR spectroscopy and imaging of biological samples, J. Magn. Reson. Ser. B 108 (1995) 67–72.
[27] G. He, S. Petryakov, A. Samoulilov, M. Chzhan, P. Kuppusamy, J.L. Zweier, Development of a resonator with automatic tuning and coupling capability to minimize sample motion noise for in vivo EPR spectroscopy, J. Magn. Reson. 149 (2001) 218–227.
[28] H. Hirata, Z.-W. Luo, Stability analysis and design of automatic frequency control system for in vivo EPR spectroscopy, Magn. Reson. Med. 46 (2001) 1209–1215;
H. Hirata, Z.-W. Luo, Stability analysis and design of automatic frequency control system for in vivo EPR spectroscopy, Erratum 49 (2003) 977.
[29] H. Sato-Akaba, H. Fujii, H. Hirata, Improvement of temporal resolution for three-dimensional continuous-wave electron paramagnetic resonance imaging, Rev. Sci. Instrum. 79 (2008) 123701.
[30] H. Sato-Akaba, Y. Kuwahara, H. Fujii, H. Hirata, Half-life mapping of nitroxyl radicals with three-dimensional electron paramagnetic resonance imaging at an interval of 3.6 seconds, Anal. Chem. 81 (2009) 7501–7506.
[31] Z.-P. Liang, P.C. Lauterbur, Principles of Magnetic Resonance Imaging: A Signal Processing Perspective, IEEE Press, Piscataway, NJ, 2000. pp. 207–209.
[32] http://rsbweb.nih.gov/ij/.
[33] C. Bowick, RF Circuit Design, Newnes, Boston, MA, 1982. pp. 37–43.
[34] T. Ogata, Y. Ishikawa, M. Ono, L.J. Berliner, Visualization of eddy-current losses in L-Band ESR imaging, J. Magn. Reson. 97 (1992) 616–622.
[35] M. Sueki, G.A. Rinard, S.S. Eaton, G.R. Eaton, Effect of eddy currents on EPR spectra, J. Magn. Reson. Ser. A 103 (1993) 208–216.
[36] B. Wu, X.L. Zhang, P. Qu, G.X. Shen, Design of an inductively decoupled microstrip array at 9.4 T, J. Magn. Reson. 182 (2006) 126–132.
[37] R.F. Lee, R.O. Giaquinto, C.J. Hardy, Coupling and decoupling theory and its application to the MRI phased array, Magn. Reson. Med. 48 (2002) 203–213.
[38] H. Yokoyama, Twin LC resonator system for EPR measurements operating at radio-frequency, Appl. Magn. Reson. 38 (2010) 501–509.